

Propagation and Signatures of Ultra High Energy Cosmic Rays

V. Berezhinsky^{a*}, A. Gazizov^b and S. Grigorieva^c

^aINFN - Laboratori Nazionali del Gran Sasso, I-67010 Assergi (AQ), Italy

^bDESY Zeuthen, Platanenallee 6, D-15738 Zeuthen, Germany

^cInstitute for Nuclear Research, Russian Academy of Sciences, 60th October Revolution Prospect 7A, 117312 Moscow, Russia

We study the extragalactic protons with universal spectrum, which is independent of mode of propagation, when distance between sources is less than the propagation lengths, such as energy attenuation length or diffusion length (for propagation in magnetic fields). The propagation features in this spectrum, the GZK cutoff, dip and bump, are studied with help of modification factor, which weakly depends on the generation spectrum index γ_g . We argue that from the above features the dip is the most model-independent one. For the power-law generation spectrum with $\gamma_g = 2.7$ the dip is very well confirmed by the data of all existing detectors, which gives the strong evidence for extragalactic protons propagating through CMB. We develop the AGN model for origin of UHECR, which successfully explains the observed spectra up to 1×10^{20} eV and transition from galactic to extragalactic cosmic rays. The calculated spectrum has the GZK cutoff, and the AGASA excess of events at $E \gtrsim 1 \times 10^{20}$ eV needs another component, e.g. from superheavy dark matter. In case of weak extragalactic magnetic fields this model is consistent with small-angle clustering and observed correlation with BL Lacs.

1. Introduction

The systematic study of Ultra High Energy Cosmic Rays (UHECR) started in late fifties after construction of Volcano Ranch (USA) and Moscow University (USSR) arrays. During next 50 years of research the origin of UHE particles, which hit the detectors, was not well understood. At present due to the data of the last generation arrays, Haverah Park (UK), Yakutsk (Russia), Akeno and AGASA (Japan), and Fly's Eye and HiRes (USA) [1] we are probably very close to understanding the origin of UHECR, and the data of Auger detector [2] will undoubtedly substantially clarify this problem.

On the theoretical side we have an important clue to understanding the UHECR origin: the interaction of extragalactic protons, nuclei and photons with CMB, which leaves the imprint on UHE proton spectrum, most notably in the form of the Greisen-Zatsepin-Kuzmin (GZK) [3] cutoff.

We shall shortly summarize the basic experimental results and the results of the data analy-

sis, important for understanding of UHECR origin (for a review see [4]).

(i) The spectra of UHECR are measured [1] with good accuracy at 1 - 100 EeV, and these data have a power to reject or confirm some models. The discrepancy between the AGASA and HiRes data at $E > 100$ EeV might have the statistical explanation [5].

(ii) The mass composition at $E \gtrsim 1$ EeV (as well as below) is badly known (for a review see [6]). The different methods give the different mass composition, and the same methods disagree in different experiments. Probably the most reliable method of measuring the mass composition is given by elongation rate (energy dependence of maximum depth of shower X_{\max}) measured by the fluorescent method. The data of Fly's Eye in 1994 [1] favored iron nuclei at 1 EeV with a gradual transition to the protons at 10 EeV. The further development of this method by the HiRes detector, which is the extension of Fly's Eye, shows the transition to the proton composition already

*Talk presented by V. Berezhinsky

at 1 EeV [7].

(iii) The arrival directions of particles with energy $E \geq 4 \times 10^{19}$ eV show the small-angle clustering within the angular resolution of detectors. AGASA found 3 doublets and one triplet among 47 detected particles [8] (see the discussion [9]). In the combined data of several arrays [10] there were found 8 doublets and 2 triplets in 92 events. The stereo HiRes data [11] do not show small-angle clustering for 27 events at $E \geq 4 \times 10^{19}$ eV, maybe due to limited statistics.

Small-angle clustering is most naturally explained in case of rectilinear propagation as a random arrival of two (three) particles from a single source [12]. This effect has been calculated in Refs. [13,14,15,16,17]. In the last four works the calculations have been performed by MC method and results agree well. According to [17] the density of the sources, needed to explain the observed number of doublets is $n_s = (1-3) \times 10^{-5} \text{ Mpc}^{-3}$. In [16] the best fit is given by $n_s \sim 1 \times 10^{-5} \text{ Mpc}^{-3}$ and the large uncertainties (in particular due to ones in observational data) are emphasized.

(iv) There have been recently found the statistically significant correlations between direction of particles with energies $(4-8) \times 10^{19}$ eV and directions to AGN of the special type - BL Lacs [18] (see also the criticism [19] and the reply [20]).

The items (iii) and (iv) favor rectilinear propagation of primaries from the point-like extragalactic sources, presumably AGN. This statement provokes many questions:

Is rectilinear propagation the only solution to clustering (e.g. does it appear in propagation of protons in strong magnetic fields)? In case the correlation with AGN is true, what are the primaries (protons in weak magnetic field or neutral particles)?

In this paper we shall analyse the origin of UHECR in two steps. In the first one we will use only most reliable observational data, namely the energy spectra and fluxes under the most conservative assumption that primaries are extragalactic protons. We shall calculate spectra for propagation in weak and reasonably strong magnetic fields, and demonstrate the strong evidence in fa-

vor of protons as the primaries at energies 1 - 80 EeV. This part of analysis is almost model independent. In the second step we shall include the data (iii) and (iv) and formulate our model. In the framework of our model we shall discuss the connection between galactic and extragalactic components of cosmic rays, and the problem with superGZK particles, i.e. ones at $E > 100$ EeV.

2. Three problems of UHECR

1. SuperGZK particles at $E \gtrsim 1 \times 10^{20}$ eV.

“The AGASA excess”, namely 11 events with energy higher than 1×10^{20} eV, cannot be explained as extragalactic protons, nuclei or photons. While the spectrum up to 8×10^{19} eV is well explained as extragalactic protons with the GZK cutoff, the AGASA excess should be described as another component of UHECR, most probably connected with the new physics: superheavy dark matter, new signal carriers, like e.g. light stable hadron and strongly interacting neutrino, the Lorentz invariance violation etc.

The problem with superGZK particles is seen in other detectors, too. Apart from the AGASA events, there are five others: the golden FE event with $E \approx 3 \times 10^{20}$ eV, one HiRes event with $E \approx 1.8 \times 10^{20}$ eV and three Yakutsk events with $E \approx 1 \times 10^{20}$ eV. No sources are observed in the direction of these particles at the distance of order of attenuation length. The most severe problem is for the golden FE event: with attenuation length $l_{\text{att}} = 21$ Mpc and the homogeneous magnetic field 1 nG on this scale, the deflection of particle is only 3.7° . Within this angle there are no remarkable sources at distance ~ 20 Mpc [21].

2. Transition from galactic to extragalactic cosmic rays.

All measurements agree with the existence of the proton knee at energy about 2.5×10^{15} eV and with increasing of the mean atomic number A of the primaries as energy grows up to 1×10^{17} eV. If the knee is due to rigidity-dependent propagation (diffusion) or rigidity-dependent acceleration, the iron nuclei should have a knee at $\sim 7 \times 10^{16}$ eV, as it is indeed observed by KASCADE (see Section 6 for the details). On the other hand, the ankle

at $E \sim 1 \times 10^{19}$ eV, discovered in late 70s in the Haverah Park data [22], is traditionally considered as transition from galactic to extragalactic cosmic rays.

How the gap between 1×10^{17} eV and 1×10^{19} eV is filled?

This problem was studied in [23]. We shall consider it in Section 6.

Acceleration to $E \gg 1 \times 10^{20}$ eV.

Acceleration to $E_{\max} \sim 1 \times 10^{21}$ eV is sufficient for present observations. It can happen that future observations, e.g. by EUSO, will indicate to considerably higher E_{\max} .

The conservative shock acceleration mechanism can provide $E_{\max} \sim 1 \times 10^{21}$ eV only for selected astrophysical objects, such as AGN [24] and GRBs [25]. However, there are many other mechanisms of accelerations which are not developed mathematically as good as the shock acceleration but which in principle can accelerate particles to much higher energies and to be very powerful. They include unipolar induction, operating in the accretion discs, jets from black holes and fast-rotating pulsars, acceleration in strong e-m waves in vacuum and plasma, and different types of plasma acceleration mechanisms (see [26] for a review). Therefore, acceleration of particles to $E \gg 1 \times 10^{20}$ eV does not look forbidden. The more restrictive problem is a presence of such accelerators nearby our galaxy or inside it. However, discovery of particles with $E \gg 1 \times 10^{20}$ eV will imply either “new” acceleration mechanisms or top-down scenarios.

One can find more discussion of UHECR problems in review [27].

3. Propagation theorem and the universal spectrum

As numerical simulations show (see e.g. [28, 29]), the propagation of UHE protons in strong magnetic fields changes the energy spectrum (for physical explanation of this effect see [30]). The influence of magnetic field on spectrum depends on the separation of the sources d . The propagation theorem reads:

For uniform distribution of sources with sepa-

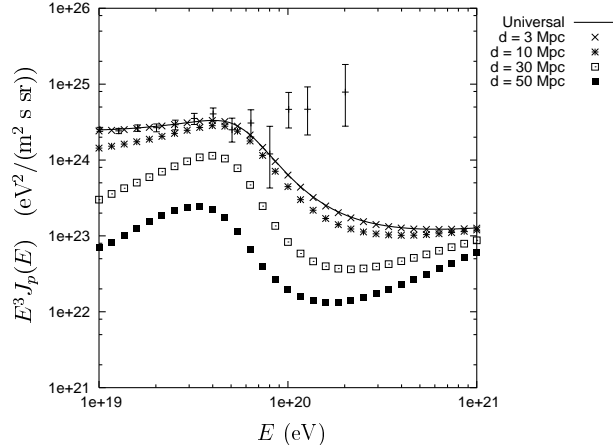


Figure 1. Convergence of the diffusive spectrum to the universal spectrum in the case of diffusion in the random magnetic fields with $(B_0, l_c) = (100 \text{ nG}, 1 \text{ Mpc})$, where B_0 is the magnetic field on the basic turbulent scale l_c . At small energies the Bohm diffusion is assumed. The data points are from AGASA.

ration much less than characteristic lengths of propagation, such as attenuation length l_{att} and the diffusion length l_{diff} , the diffuse spectrum of UHECR has an universal (standard) form independent of mode of propagation.

For the proof see [30]. We shall illustrate this theorem by convergence of the spectrum calculated in the diffusion approximation to the *universal* spectrum (see below), when the distance between sources, d , becomes small. In Fig. 1 the diffuse spectra are calculated in the diffusion approximation for the strong magnetic field (100 nG on the basic scale 1 Mpc) for different distances between sources indicated in the figure. The universal spectrum is shown by the solid line. All spectra correspond to the same emissivity \mathcal{L} . For $d = 50$ Mpc the diffusive spectrum (black boxes) is quite different from the universal one. When $d = 10$ Mpc (stars) both spectra are very similar, and at $d = 3$ Mpc (crosses) they become indistinguishable. In the case of the reasonable fields, 1 - 10 nG, the diffusive spectra are universal for all reasonable separations d .

Universal spectrum.

One can calculate the spectrum from conservation

of number of particles in the comoving volume (protons change their energy but do not disappear). For the number of UHE protons per unit comoving volume, $n_p(E)$, one has:

$$n_p(E)dE = \int_0^{t_0} dt Q_{\text{gen}}(E_g, t) dE_g, \quad (1)$$

where t is an age of the universe, $E_g = E_g(E, t)$ is a generation energy at age t , $Q_{\text{gen}}(E_g, t)$ is the generation rate per unit comoving volume, which can be expressed through emissivity \mathcal{L}_0 , the energy release per unit time and unit of comoving volume at $t = t_0$, as

$$Q_{\text{gen}}(E_g, t) = \mathcal{L}_0(1+z)^m K q_{\text{gen}}(E_g), \quad (2)$$

where $(1+z)^m$ describes possible cosmological evolution of the sources. In the case of the power-law generation, $q_{\text{gen}}(E_g) = E_g^{-\gamma_g}$, with normalization constant $K = \gamma_g - 2$ for $\gamma_g > 2$.

From Eq.(1) one obtains the diffuse flux as

$$J_p(E) = \frac{c}{4\pi} \mathcal{L}_0 K \times \int_0^{z_{\text{max}}} dz \frac{dt}{dz} (1+z)^m q_{\text{gen}}(E_g) \frac{dE_g}{dE}, \quad (3)$$

where

$$dt/dz = \left[H_0(1+z) \sqrt{\Omega_m(1+z)^3 + \Omega_\Lambda} \right]^{-1}; \quad (4)$$

analytic expression for dE_g/dE is given in [31].

The spectrum (3) is referred to as *universal spectrum*. Formally it is derived from conservation of particles and does not depend from propagation mode (see Eq. (1)). But in fact, the homogeneity of the particles, tacitly assumed in this derivation, implies the homogeneity of the sources, and thus the condition of validity of universal spectrum is a small separation of sources. The homogeneous distribution of particles in case of homogeneous distribution of sources and *inhomogeneous* magnetic fields follows from the Liouville theorem (see Ref. [30]).

4. Spectrum features from proton interaction with CMB

The extragalactic protons propagating through CMB produce signatures in the form of three

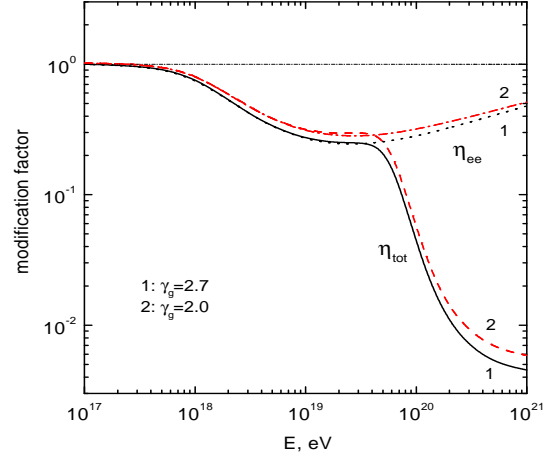


Figure 2. Modification factor for the power-law generation spectra with γ_g in a range 2.0 -2.7. Curve $\eta = 1$ corresponds to adiabatic energy losses only, curves η_{ee} corresponds to adiabatic and pair production energy losses and curves η_{tot} - to all energy losses included.

spectrum features: GZK cutoff, dip and bump. The dip is produced due to e^+e^- -production and bump – by pile-up protons accumulated near beginning of the GZK cutoff.

The analysis of these features is convenient to perform in terms of *modification factor* [32,33].

Modification factor is defined as a ratio of the spectrum $J_p(E)$, with all energy losses taken into account, to unmodified spectrum J_p^{unm} , where only adiabatic energy losses (red shift) are included.

$$\eta(E) = \frac{J_p(E)}{J_p^{\text{unm}}(E)}. \quad (5)$$

For the power-law generation spectrum one has

$$J_p^{\text{unm}} = \frac{c}{4\pi} (\gamma_g - 2) \mathcal{L}_0 E^{-\gamma_g} \int_0^{z_{\text{max}}} dz \frac{dt}{dz} (1+z)^{-\gamma_g+1}$$

Modification factor is less model-dependent quantity than the spectrum. In particular, it should depend weakly on γ_g , because both numerator and denominator in Eq. (5) include $E^{-\gamma_g}$. Further on we shall consider the non-evolutionary case $m = 0$. The modification factor in Fig. 2, as expected, depends weakly on γ_g , but the shape

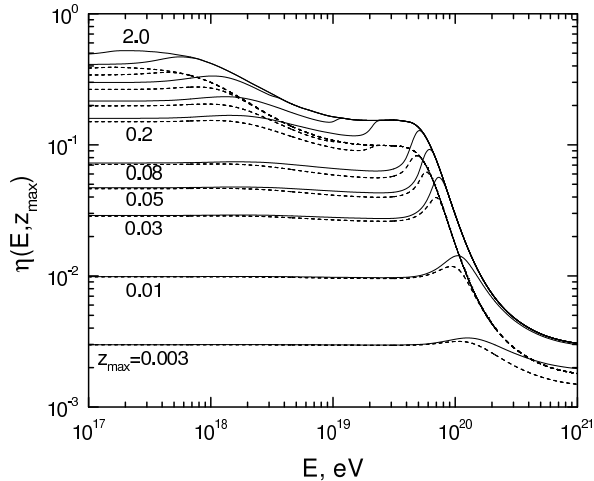


Figure 3. Disappearance of bumps in diffuse spectra (from Ref. [32]). The sources are distributed uniformly in the sphere of radius R_{max} , corresponding to z_{max} . The solid and dashed curves are for $\gamma_g = 2.7$ and $\gamma_g = 2.0$, respectively. The curves between $z_{\text{max}} = 0.2$ and $z_{\text{max}} = 2.0$ have $z_{\text{max}} = 0.3, 0.5, 1.0$.

of the GZK cutoff is strongly model-dependent: it is more flat in case of local overdensity of the sources, and more steep in case of their local deficit.

The dip is a more reliable signature of interaction of protons with CMB: its shape is fixed and has rather complicated form to be imitated by other mechanism. The protons in the dip are collected from the large volume with the linear size about 1000 Mpc and therefore the assumption of uniform distribution of sources within this volume is well justified. In contrast to this well predicted and specifically shaped feature, the cutoff, if discovered, can be produced as the acceleration cutoff (steepening below E_{max}). Since the shape of both, GZK cutoff and acceleration cutoff, is model-dependent, it will be difficult to argue in favor of any of them. The problem of identification of the dip depends on the accuracy of observational data, which should confirm the complicated shape of this feature. Do the present data have the needed accuracy? We shall address to this question in the next Section.

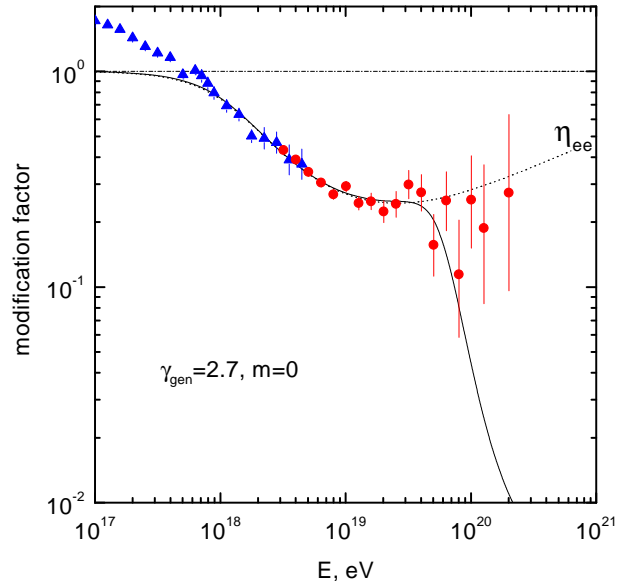


Figure 4. Predicted dip in comparison with the Akeno-AGASA data.

Let us now come over to the bump. We see no indication of the bump in Fig. 2 at merging of $\eta_{ee}(E)$ and $\eta_{\text{tot}}(E)$ curves, where it should be located. The absence of the bump in the *diffuse spectrum* can be easily understood. The bump is clearly seen in the spectrum of a single remote source [32,33]. These bumps, located at different energies, produce a flat feature, when they are summed up in the diffuse spectrum. This effect can be illustrated by the Fig. 3 from Ref. [32]. In Fig. 3 the diffuse flux is calculated in the model where sources are distributed uniformly in the sphere of radius R_{max} (or z_{max}). When z_{max} are small (between 0.01 and 0.1) the bumps are seen in the diffuse spectra. When radius of the sphere becomes larger, the bumps merge producing the flat feature in the spectrum. If the diffuse spectrum is plotted as $E^3 J_p(E)$ this flat feature looks like a pseudo-bump.

5. Dip as the signature of proton interaction with CMB

The comparison of the calculated modification factor with that obtained from the Akeno-AGASA data, using $\gamma_g = 2.7$, is shown in Fig. 4.

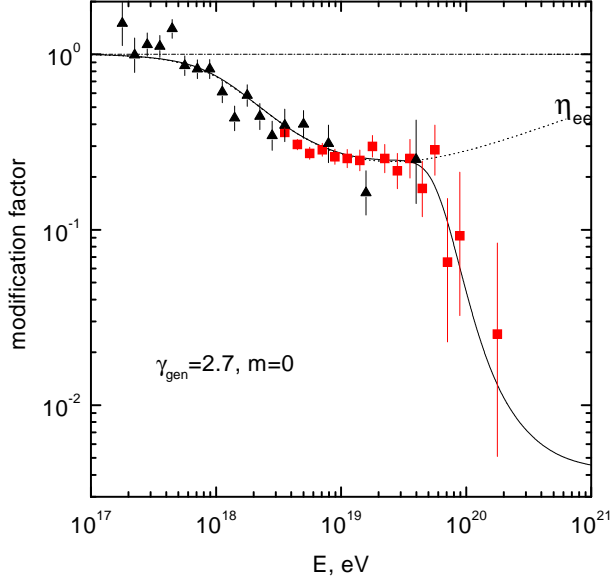


Figure 5. Predicted dip in comparison with the HiRes data.

From Fig. 4 one observes the excellent agreement of predicted and observed modification factors for the dip. By definition $\eta(E) \leq 1$. In Fig. 4 one sees that at $E \leq 4 \times 10^{17}$ $\eta_{\text{obs}} > 1$. It signals about appearance of another component of cosmic rays, which is most probably galactic cosmic rays. The condition $\eta > 1$ means the dominance of the new (galactic) component, the transition occurs at higher energy.

To calculate χ^2 for the confirmation of the dip by Akeno-AGASA data, we choose the energy interval between 1×10^{18} eV (which is somewhat arbitrary in our analysis) and 4×10^{19} eV (the energy of intersection of $\eta_{ee}(E)$ and $\eta_{\text{tot}}(E)$). In calculations we used the Gaussian statistics for low-energy bins, and the Poisson statistics for the high energy bins of AGASA. It results in $\chi^2 = 19.06$. The number of Akeno-AGASA bins is 19. We use in calculations two free parameters: γ_g and the total normalization of spectrum. In effect, the confirmation of the dip is characterised by $\chi^2 = 19.06$ for d.o.f=17, or $\chi^2/\text{d.o.f}=1.12$.

In Fig. 5 the comparison of modification factor with the HiRes data is shown. The agreement is also good.

The good agreement of the shape of the dip

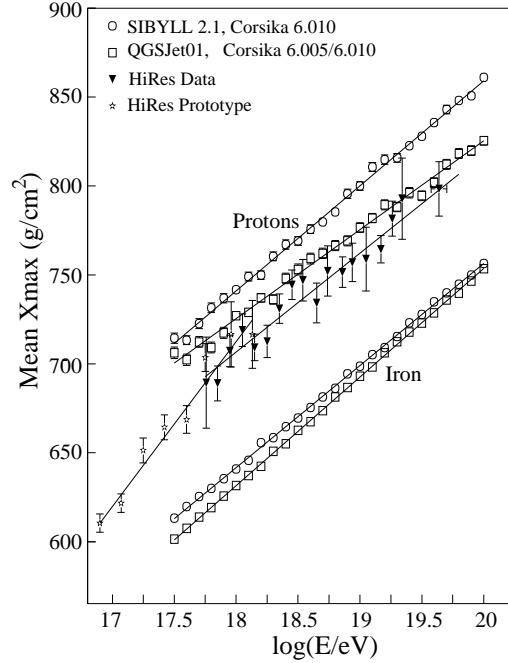


Figure 6. The HiRes data [7] on the mass composition. The measured X_{max} at $E \geq 1 \times 10^{18}$ eV are in a good agreement with the QGSJet-Corsika prediction for protons.

$\eta_{ee}(E)$ with observations is a strong evidence for extragalactic protons interacting with CMB. This evidence is confirmed by the HiRes data on the mass composition, which favor the protons (see Fig. 6).

6. AGN model

We will consider the AGN model phenomenologically, i.e. not specifying the acceleration mechanism and assuming that space density of AGN satisfies the universal spectrum. The data on small-angle clustering and correlation with AGN will be involved in the analysis. We shall consider density of the sources and their luminosities, spectra, transition from galactic to extragalactic cosmic rays and the problem of superGZK particles.

Spectra.

We will calculate the extragalactic proton spectra following ref. [34,35], in the model with the follow-

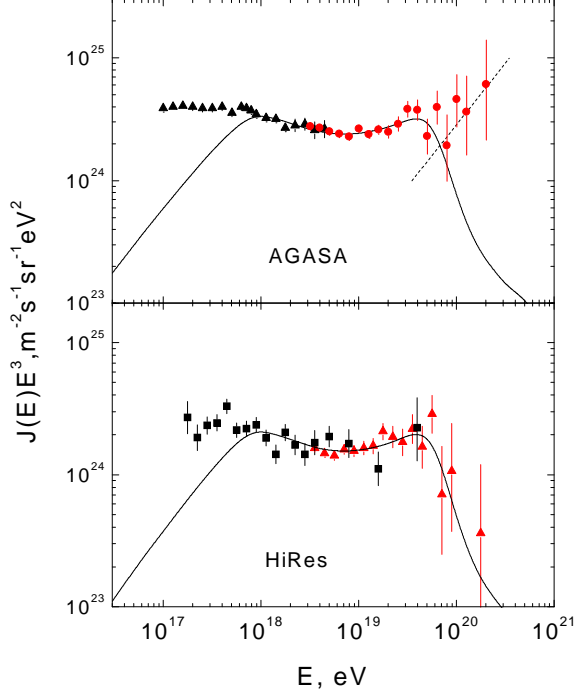


Figure 7. Comparison of calculated spectra with the data of AGASA and HiRes.

ing assumptions. We assume the generation spectrum of a source as the standard one, $\propto 1/E^2$, up to energy E_c , and more steep, $\propto 1/E^{-\gamma_g}$ at higher energies. This complex spectrum might imply two mechanisms of acceleration: the shock acceleration with $E_{\max} \lesssim E_c$ and some other mechanism working at higher energies. Thus, the generation function in Eq. (2) is determined by the following q_{gen} :

$$q_{\text{gen}}(E_g) = \begin{cases} 1/E_g^2 & \text{at } E_g \leq E_c \\ E_c^{-2}(E_g/E_c)^{-\gamma_g} & \text{at } E_g \geq E_c, \end{cases} \quad (6)$$

with normalization constant K given by

$$1/K = \ln(E_c/E_{\min}) + 1/(\gamma_g - 2). \quad (7)$$

The diffuse flux is given by Eq. (3).

We consider the non-evolutionary model, $m = 0$, with $\gamma_g = 2.7$, with $E_c \sim 1 \times 10^{18}$ eV and with most conservative maximum acceleration energy $E_{\max} = 1 \times 10^{21}$ eV. The calculated spectra are presented in Figs. 7 and 8 in comparison with the data of AGASA, Fly's Eye, HiRes and

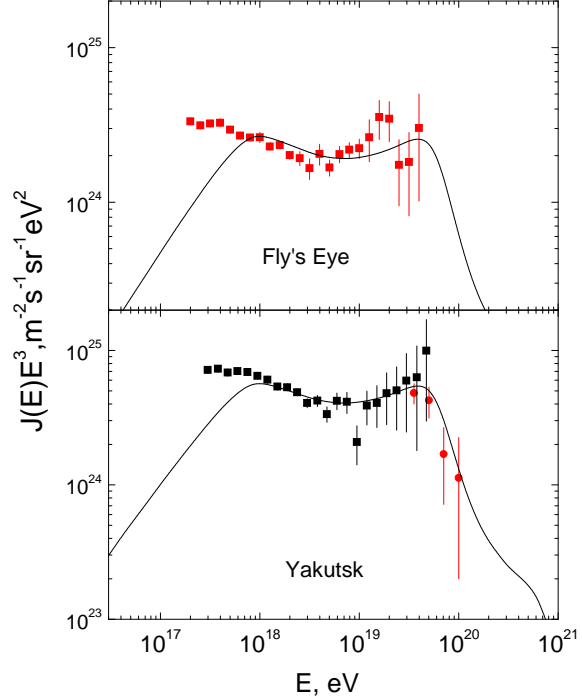


Figure 8. Comparison of calculated spectra with the data of Fly's Eye and Yakutsk.

Yakutsk arrays. The normalization of all spectra needs somewhat different emissivity \mathcal{L}_0 . The normalization to the AGASA data is given by $\mathcal{L}_0 = 3.5 \times 10^{46}$ erg/Mpc³yr. As Fig. 9 shows, the Akeno-AGASA and HiRes I - HiRes II data agree in the spectrum and flux, when the energies are shifted by the factors $\lambda = 0.9$ and $\lambda = 1.26$ for the AGASA and HiRes data, respectively. Such shift is allowed by systematic errors in energy determination for each detector. The joint spectrum is fitted well by the calculations with $\mathcal{L}_0 = 3.1 \times 10^{46}$ erg/Mpc⁻³yr. However, at $E \geq 1 \times 10^{20}$ eV there is substantial disagreement in the data of both detectors. Statistical significance of this contradiction was not evaluated by the collaborations of both experiments. This problem will be resolved soon by the Auger detector.

Transition to the galactic cosmic rays.

In agreement with all other measurements, the KASCADE data (see Fig. 10) show the gradual

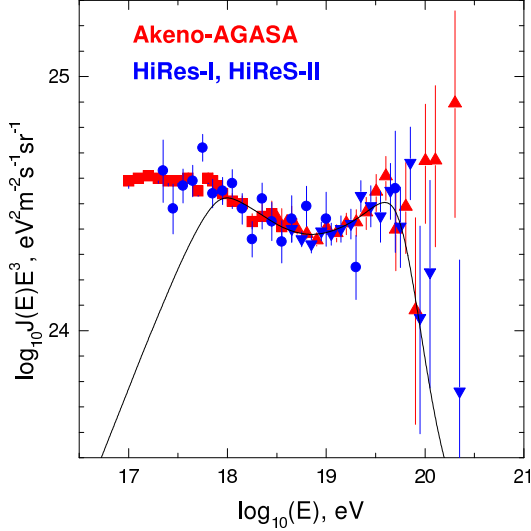


Figure 9. Agreement between the Akeno-AGASA data and HiRes I - HiRes II data when energies are shifted as $\lambda_{AGASA} = 0.9$ and $\lambda_{HiRes} = 1.26$. The combined data agree with calculations at $E \lesssim 1 \times 10^{20}$ eV. At higher energies the discrepancy remains.

transition to heavy nuclei at energies above the proton knee $E_p = 2.5 \times 10^6$ GeV. The KASCADE data are in a reasonable agreement with rigidity-propagation models or rigidity-acceleration models, according to which the positions of nuclei knees are given by $E_Z = ZE_p$, shown in Fig. 10 by vertical arrows. According to this picture, after the iron knee, $E_{Fe} = 6.5 \times 10^7$ GeV, the CR flux should decrease steeply with energy, as $E^{-\gamma_g}/D(E)$ in the rigidity-propagation models, where $D(E)$ is the diffusion coefficient in the galaxy. The all-particle KASCADE-Akeno spectrum in Fig. 10 does not show this steepening, and we interpret it as the compensation of the flux by extragalactic protons, which become the dominant component at $E \gtrsim E_c \sim 1 \times 10^9$ GeV. If transition from galactic to extragalactic component occurs at $E \sim E_c \sim 1 \times 10^9$ GeV, it should reveal itself as a *faint* feature in all-particle spectrum, because both components, galactic and extragalactic, have similar spectra. Indeed, the difference between spectral indices of the all-particle Akeno spectrum and extragalactic proton spectrum of our model is equal to $\Delta\gamma \approx 0.3$.

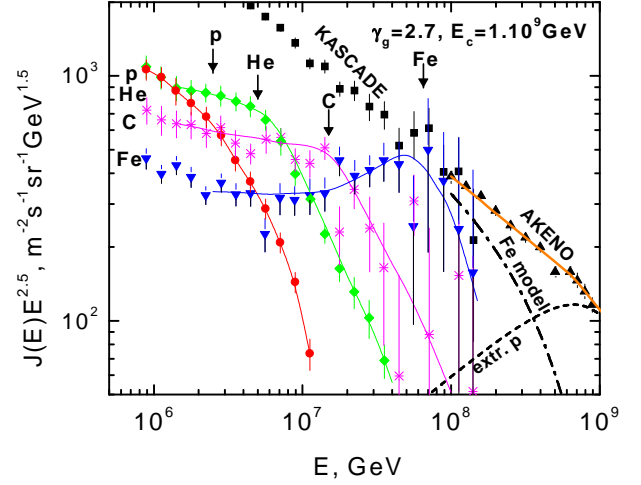


Figure 10. Predicted iron nuclei spectrum (curve Fe model) and KASCADE data [36]. The data are shown: for protons - by filled circles, for helium - by diamonds, for carbon - by stars, for iron - by inverted triangles, and for all-particle spectrum - by filled squares. The arrows labelled by p, He, C and Fe show the positions of corresponding knees, calculated as $E_Z = ZE_p$, with $E_p = 2.5 \times 10^6$ GeV. The all-particle spectrum of Akeno is shown by filled triangles.

Such faint spectral feature is well known. It is the *second knee*, whose position varies from 4×10^8 GeV to 8×10^8 GeV in different experiments (Fly's Eye - 4×10^8 GeV, Akeno - 6×10^8 GeV, HiRes - 7×10^8 GeV and Yakutsk - 8×10^8 GeV). The second knee in the Akeno spectrum is seen in Fig. 11.

Assuming that the total flux at $E \gtrsim 1 \times 10^8$ GeV is given by galactic iron nuclei and extragalactic protons, we calculated [35] the flux of galactic iron nuclei, subtracting the flux of extragalactic protons, as given by our model, from all-particle spectrum of Akeno. The resulting spectra of iron nuclei are shown in Fig. 10 for $E_c = 1 \times 10^9$ GeV and for three values of E_c in Fig. 11. The latter spectra are not exactly power-law, but in the power-law approximation they can be roughly characterised by $\gamma \approx 3.9$ for spectrum 1', $\gamma \approx 3.4$ for spectrum 2', and $\gamma \approx 3.3$ for spectrum 3'. These spectra, especially 2' and 3' are

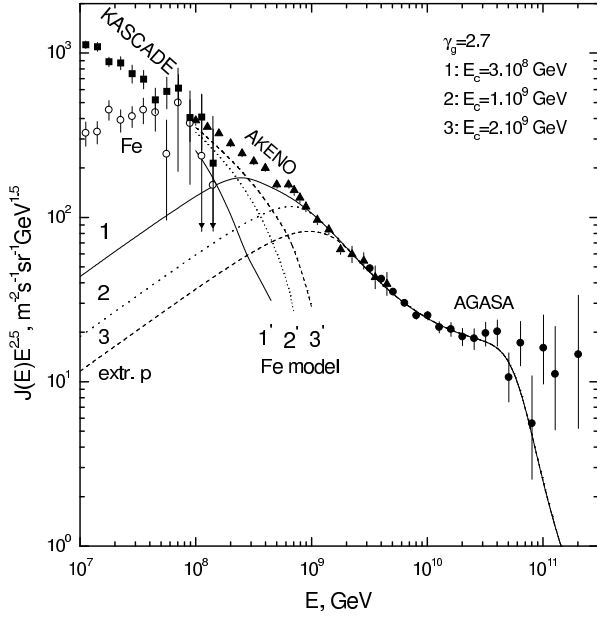


Figure 11. Calculated spectrum of extragalactic protons (curves 1, 2, 3) and of galactic iron spectra (curves 1', 2', 3') compared with all-particle spectrum from Akeno and AGASA experiments. The intersections of the curves 1 – 1', 2 – 2' and 3 – 3' give the transition from galactic (iron) to extragalactic (proton) components. The KASCADE data are shown by filled squares for all-particle fluxes and by open circles - for iron nuclei fluxes.

consistent with the Hall diffusion, which predicts $\gamma = 3.35$ (see [35]).

From Fig. 11 one can see, that while transition from the galactic to extragalactic component in all-particle spectrum is characterised by a faint feature, this transition is quite sharp when the iron and proton spectra are resolved (the intersection of curves 1' – 1, 2' – 2 and 3' – 3).

The fraction of iron in the total flux decreases as energy increases from 1×10^{17} eV to 1×10^{18} eV, changing from about 80% to $\sim 10\%$ (the predicted fraction depends on E_c , see [35]).

An interesting prediction of [35] is the visibility of galactic sources at $E \gtrsim 1 \times 10^{18}$ eV. If galactic sources accelerate particles to energies higher than 1×10^{18} eV, their “direct” flux can

be seen, while the produced diffuse flux should be small, because of short confinement time in the galaxy. If generation spectrum is dominated by protons, the “direct” flux must be seen as the protons, while the diffuse galactic flux is presented by heaviest nuclei. Due to multiple scattering of protons in the magnetic fields, the galactic point sources should be observed as the extensive sources with typical angular size $\sim 20^\circ$ at distance $r \gtrsim 10$ kpc. At higher energies and smaller distances these sources are seen as the point-like ones.

SuperGZK particles from SHDM

As Figs. 7 and 8 show, the spectrum of our model agrees with the HiRes, Yakutsk and Fly’s Eye data, but does not agree with the AGASA data at $E \geq 1 \times 10^{20}$ eV. The AGASA excess needs for its explanation another component. We will discuss here UHECR from superheavy dark matter (SHDM) as a possible candidate (see also [37]).

SHDM as a source of UHECR without GZK cutoff has been suggested and studied in Refs. [38]. SHDM is comprised by quasi-stable particles with masses $10^{13} - 10^{14}$ GeV. They are efficiently produced at post-inflationary epoch (for the review see [39]). X-particles are accumulated in the galactic halo with overdensity $\sim 2 \times 10^5$, and this effect provides the absence of the GZK cutoff.

The spectra of particles produced in X-particle decay have been recently reliably calculated by three independent groups and by two different methods [40,41]. As the main results, these calculations give almost power-law spectrum $\propto E^{-\gamma}$ with $\gamma = 1.94$ and the increased ratio of nucleons to photons $N/\gamma \approx 0.33 - 0.50$ [41].

With this spectrum the SHDM model can explain only the AGASA excess at $E \gtrsim 1 \times 10^{20}$ eV, as shown in Fig. 12.

There are two main signatures of UHECR from SHDM:

- (i) The dominance of primary photons with ratio $\gamma/p \approx 2 - 3$.
- (ii) Excess of particles from the direction of the Galactic Center.

The first signature has been studied recently [42], using the AGASA data. Note, that only events

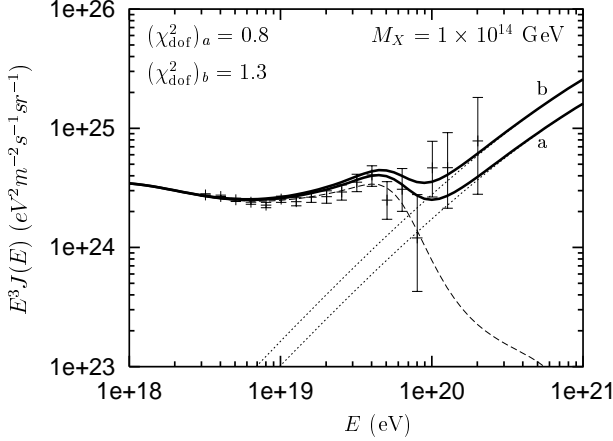


Figure 12. The universal spectrum (dashed curve) and spectra from SHDM (dotted curves) [41], in comparison with AGASA data. The SHDM spectra are shown for two normalizations. The sum of two components is shown by the thick solid curves. The χ^2 values are given for the comparison of these two curves with the AGASA data at $E \geq 4 \times 10^{19}$ eV.

with $E \gtrsim 1 \times 10^{20}$ eV are relevant. The recent theoretical prediction, $p/\gamma = 0.33 - 0.50$, substantially changes the conclusions of [42].

From 11 events at $E \geq 1 \times 10^{20}$ eV, muons were detected only in 6 showers: 4 with two muon detectors fired (cut A) and 2 more with one muon detector fired (cut B) (are other 5 showers muon-poor or muon signal in the detectors are absent due to fluctuations?). From Fig. 2 of Ref. [42] one sees only two events (cut A), where muon content contradicts to photon-induced showers, with two more which are marginally consistent with photon-induced showers, and with two more located in the zone allowed for the photon-induced showers. With p/γ ratio given above the number of proton-induced showers is predicted to be 2.75 - 3.63 in a good agreement with 2 (or even 4) showers with the hadronic muon content. As to arrival distribution with account of geomagnetic absorption and LPM suppression of showers from unabsorbed photons, we think that more detailed theoretical calculations and better statistics is needed for the reliable conclusions. However, we agree with the final conclusion of the paper [42]: “Above 10^{20} eV no indication of γ -ray

dominance is found in both $\rho_\mu(1000)$ and arrival direction distributions”.

The second signature (ii) is reliably predicted (it is caused by DM distribution in the halo) and will be tested soon by the Auger detector. The absence of anisotropy centered by the Galactic Center excludes the SHDM model as explanation of the AGASA excess.

AGN as UHECR sources.

We will accept here the MHD simulation [43] of magnetic fields in various universe structures. These simulations favor relatively weak magnetic fields in the structures, namely of the order of 0.1 nG in typical filaments and of 0.01 nG in the voids, the magnetic field in the Local Universe is also weak (notice, however, the simulations [44] in which stronger magnetic fields are obtained). With magnetic fields from simulations [43], protons with $E > 4 \times 10^{19}$ eV propagate quasi-rectilinearly and the small-angle clustering is most naturally explained with the density of the sources given [17,16] as

$$n_s \sim (1 - 3) \times 10^{-5} \text{ Mpc}^{-3}, \quad (8)$$

with some uncertainties as indicated in [16]. Correlation with BL Lacs [18] indicates directly to AGN as the sources of UHECR.

With $n_s = 3 \times 10^{-5} \text{ Mpc}^{-3}$ and $\mathcal{L}_0 = 3.5 \times 10^{46} \text{ erg/Mpc}^3\text{yr}$, the CR-luminosity of a source is $L_p = \mathcal{L}_0/n_s = 3.7 \times 10^{43} \text{ erg/s}$. Both n_s and L_p correspond well to relatively powerful AGN.

In vicinity of Milky Way at redshift $z \leq 0.009$, or $r \leq 38 \text{ Mpc}$, there are 12 AGN, including such powerful Seyferts as NGC 4051, NGC 4151, NGC 1068 and radiogalaxy Cen A. It corresponds to density $n_s = 5 \times 10^{-5} \text{ Mpc}^{-3}$, consistent with the density above. At redshift $z \leq 0.0167$ ($r \leq 70.6 \text{ Mpc}$), there are 19 Seyferts and radiogalaxies which results in $n_s = 1.3 \times 10^{-5} \text{ Mpc}^{-3}$, also in agreement with the discussed density. We will remind that attenuation length of proton with $E = 1 \times 10^{20} \text{ eV}$ is 135 Mpc, and with $E = 2 \times 10^{20} \text{ eV}$ is 32 Mpc. The Auger detector with large statistics at $E \gtrsim 1 \times 10^{20} \text{ eV}$ will have the good chances to observe some of these

sources.

Acceleration.

In Eq. (6) we assumed the generation spectrum as $\propto 1/E^2$ at $E \leq E_c$ and $\propto E^{-2.7}$ at $E \geq E_c$ with $E_c \sim 1 \times 10^{18}$ eV. This spectrum implies two mechanisms of acceleration. The shock acceleration responsible for the standard $1/E^2$ spectrum has $E_{\max} < E_c$. The second (hypothetical) mechanism is assumed to work at $E > E_{\min} \sim E_c$. As a result, the generation spectrum has some feature near $E \sim E_c$, which we very approximately describe by Eq. (6). The second component can be due to acceleration in the jet. A pinch acceleration mechanism which works in jet plasma was suggested in [45]. Particles are accelerated with spectrum $Q(E) \propto E^{-\gamma_g}$, where $\gamma_g = 1 + \sqrt{3} = 2.73$, i.e. exactly as we assume. The maximum energy is connected with maximum current at discharge $E_{\max} = (2e/c)I_{\max}$ and can be higher than 1×10^{21} eV.

7. Conclusions

We developed the most conservative scenario for the observed UHECR as extragalactic protons.

There are three signatures of UHE protons propagating through CMB: GZK cutoff, bump and dip. While bump is argued to be absent in the diffuse spectra and presence of the GZK cutoff is questioned by the AGASA data, the dip is confirmed with very good accuracy by the AGASA and HiRes data (see Figs. 4, 5).

The predictions for the dip in terms of modification factor are very weakly model-dependent: its shape varies but little with γ_g in the interval 2.0 – 2.7, the assumption of homogeneity in distribution of the sources is well justified, because UHE protons are collected from the large distances of order $l_{\text{att}} \sim 1000$ Mpc, and its shape is valid for both weak and reasonably strong magnetic fields. For conversion of the observed spectra into modification factor two free parameters are needed: γ_g and normalization. For 19 energy bins of the Akeno-AGASA data and two free parameters, the agreement is characterised by $\chi^2 = 19.06$ and $\chi^2/\text{d.o.f.} = 1.12$ for d.o.f.=17.

Modification factor must satisfy $\eta \leq 1$. At $E \leq 4 \times 10^{17}$, as Fig. 4 shows, $\eta > 1$, which signals about appearance of galactic CR component at energy higher, but not much than given above. This conclusion agrees with recent data of HiRes (see Fig. 6) which show that proton component becomes dominant at $E \gtrsim 1 \times 10^{18}$ eV.

In our model we assume AGN as the sources, with generation spectrum given by Eq. (6). With emissivity $\mathcal{L}_0 \approx 3.5 \times 10^{46}$ erg/Mpc³yr this spectrum describes well the AGASA, HiRes, Fly's Eye and Yakutsk data. The galactic flux of iron nuclei, calculated in energy range $1 \times 10^{17} - 1 \times 10^{18}$ eV from extragalactic flux of our model and all-particle Akeno spectrum agrees well with iron-nuclei flux measured by KASCADE. The spectrum shape is consistent with the Hall diffusion.

Our spectrum has the GZK cutoff and it is consistent with HiRes, Fly's Eye and Yakutsk data. For the explanation of the AGASA excess at $E \gtrsim 1 \times 10^{20}$ eV another component of UHECR is needed. In this paper we discuss UHECR from SHDM as such component. The calculated spectrum agrees well with observations. We argue that with predicted ratio of primary photons to protons $\gamma/p \approx 2 - 3$, SHDM does not contradict the AGASA observations [42].

Acknowledgements

We are grateful to our coauthors, Roberto Aloisio and Bohdan Hnatyk, for the pleasure of the joint work and for many fruitful discussions.

REFERENCES

1. M. Takeda *et al.* [AGASA collaboration], astro-ph/0209422; N. Hayashida *et al.* [AGASA collaboration], Phys. Rev. Lett. **73**, 3491 (1994); K. Shinozaki *et al.* [AGASA collaboration], Astrophys. J. **571**, L117 (2002); T. Abu-Zayyad *et al.* [HiRes collaboration], astro-ph/0208243; D. J. Bird *et al.* [Fly's Eye collaboration], Ap. J. **424**, 491 (1994); A. V. Glushkov *et al.* [Yakutsk collaboration], JETP Lett. **71**, 97 (2000); M. Ave *et al.* [Haverah Park collaboration], Astrop. Phys. **19**, 61 (2003).

2. J. W. Cronin, Proceedings of ICRC 2001.
3. K. Greisen, Phys. Rev. Lett. **16**, 748 (1966); G. T. Zatsepin and V. A. Kuzmin, JETP Lett. **4**, 78 (1966).
4. M. Nagano and A. Watson, Rev. Mod. Phys. **72**, 689 (2000).
5. D. De Marco, P. Blasi and A. Olinto, Astrop. Phys. **20**, 53 (2003).
6. A. Watson, these Proceedings.
7. G. Archbold and P. V. Sokolsky, Proc. of 28th International Cosmic Ray Conference, 405 (2003); G. Thompson, These Proceedings.
8. M. Takeda [AGASA collaboration], Ap. J. **522**, 225 (1999).
9. C. B. Finley and S. Westerhoff, Astrop. Phys. **21**, 359 (2004).
10. Y. Uchihori et al., Astrop. Phys. **13**, 151 (2000).
11. R. U. Abbasi et al., astro-ph/0404137.
12. S. L. Dubovsky, P. G. Tinyakov and I. I. Tkachev, Phys. Rev. Lett. **85**, 1154 (2000).
13. Z. Fodor and S. Katz, Phys. Rev. D **63**, 23002 (2001).
14. H. Yoshiguchi, S. Nagataki, K. Sato, Ap. J. **592**, 311 (2003).
15. H. Yoshiguchi, S. Nagataki, K. Sato, astro-ph/0404411.
16. P. Blasi and D. De Marco, Astrop. Phys. **20**, 559 (2004).
17. M. Kachelriess and D. Semikoz, astro-ph/0405258.
18. P. G. Tinyakov and I. I. Tkachev, JETP Lett. **74**, 445 (2001).
19. N. W. Evans, F. Ferrer and S. Sarkar, Phys. Rev. D **69**, 128302 (2004).
20. P. G. Tinyakov, I. I. Tkachev, astro-ph/0301336.
21. J. W. Elbert and P. Sommers, Ap. J. **441**, 151 (1995).
22. G. Cunningham et al, Ap. J. **236**, L75 (1980).
23. J. R. Hoerandel, Astroparticle Phys. **19**, 193 (2003).
24. P. L. Biermann and P. A. Strittmatter, Ap. J. **322**, 643 (1987).
25. E. Waxman, Phys. Rev. Lett. **75**, 386 (1995); M. Vietri, Ap. J. **453**, 883 (1995).
26. V. S. Berezhinsky, S. V. Bulanov, V. A. Dogiel, V. L. Ginzburg and V. S. Ptuskin, Astrophysics of Cosmic Rays, North-Holland 1990.
27. A. V. Olinto, Phys. Rep. **333**, 329 (2000).
28. G. Sigle, M. Lemoine and P. Biermann, Astrop. Phys. **10**, 141 (1999).
29. H. Yoshiguchi et al, Ap. J. **586**, 1211 (2003).
30. R. Aloisio and V. Berezhinsky, astro-ph/0403095.
31. V. Berezhinsky, A. Z. Gazizov, S. I. Grigorieva, hep-ph/0204357.
32. V. S. Berezhinsky and S. I. Grigorieva, Astron. Astroph. **199**, 1 (1988).
33. T. Stanev et al, Phys. Rev. D **62**, 093005 (2000).
34. V. Berezhinsky, A. Z. Gazizov, S. I. Grigorieva, astro-ph/0210095.
35. V. Berezhinsky, S. I. Grigorieva, B. I. Hnatyk, astro-ph/0403477.
36. K.-H. Kampert et al (KASCADE-Collaboration), Proceedings of 27th ICRC, volume "Invited, Rapporteur, and Highlight papers of ICRC", 240 (2001).
37. R. Aloisio, These Proceedings.
38. V. Berezhinsky, M. Kachelrieß and A. Vilenkin, Phys. Rev. Lett. **79**, 4302 (1997); V. A. Kuzmin and V. A. Rubakov, Phys. At. Nucl. **61**, 1028 (1998); M. Birkel, S. Sarkar, Astropart. Phys. **9**, 297-309 (1998); V. Berezhinsky, P. Blasi, A. Vilenkin, Phys. Rev. D **58**, 103315 (1998).
39. V. A. Kuzmin and I. I. Tkachev, Phys. Rep. **320**, 199 (1999); V. Berezhinsky, Nucl. Phys. (Proc. Suppl.) **B 87**, 387 (2000).
40. V. Berezhinsky and M. Kachelriess, Phys. Rev. D **63**, 034007 (2001); S. Sarkar and R. Toldra, Nucl. Phys. B **621**, 495 (2002); C. Barbot and M. Drees, Phys. Lett. B **533**, 107 (2002);
41. R. Aloisio, V. Berezhinsky and M. Kachelrieß, Phys. Rev. **D69**, 094023 (2004).
42. K. Shinozaki et al. (AGASA collaboration), Ap. J. **57**, L117 (2002).
43. K. Dolag, D. Grasso, V. Springel, I. Tkachev, astro-ph/0310902.
44. G. Sigl, F. Miniati, T. A. Ensslin, Phys. Rev. D **68**, 043002 (2003); G. Sigl, F. Miniati, T. A. Ensslin, astro-ph/0401084.
45. V. V. Vlasov, S. K. Zhdanov, B. A. Trubnikov, Plasma Physics **16**, 1457 (1990).